FATIGUE LIFE PREDICTION OF TITANIUM ALLOYS EFFECTED BY PROCESS FACTORS

Oleg M. Herasymchuk,[a] O. V. Kononuchenko,[a] Olena M. Herasymchuk,[b]   UDC 539.432; 620.191
and V. I. Bondarchuk[c]

A fatigue life prediction model, including stress concentrations and a microstructure of the material, is proposed. The calculations by the proposed model were compared with fatigue test results for electron beam physical vapor-deposited Ti–6Al–4V condensate specimens.

Keywords: fatigue life prediction model, stress concentration, microstructure of the material.

    Introduction. The model of life calculation to the initiation of a fatigue crack at regular symmetrical uniaxial high-cycle loads of smooth specimens was presented in [1]. The model is applicable for the materials wherein a fatigue crack originates along the stable slip band in the surface grain. The latter was obtained through modifying the Chan model [2], it provides calculations of the fatigue life N_d to the initiation of a microstructurally short crack (MSC) one grain size d deep on the basis of tensile test results and microstructure analysis of the initial material. The model [1] takes the form

$$N_d = \beta^2 \big/ (\sigma_a - \sigma_{-1})^2. \tag{1}$$

Here

$$\beta = 80 \frac{EM\zeta}{(1+\mu)^3 \sqrt{\pi(1-\mu)}}, \tag{2}$$

where ζ is the disorientation parameter,

$$\zeta = \left(\frac{Y}{2} \sqrt{S_1^2 + S_2^2} - 1 \right)^2, \tag{3}$$

$$S_1 = \cos^3 \frac{\theta_1}{2} + 3\sin \frac{\theta_1}{2} \cos^2 \frac{\theta_1}{2}, \tag{4}$$

$$S_2 = \sin \frac{\theta_1}{2} \cos^2 \frac{\theta_1}{2} - \cos \frac{\theta_1}{2} \left(1 - 3\sin^2 \frac{\theta_1}{2} \right), \tag{5}$$

$$M = \frac{1}{\cos \varphi \cos \gamma}, \tag{6}$$

M is the Taylor factor for the surface grain wherein MSC originates, φ is the slip plane normal–load direction angle, γ is the slip direction–load direction angle, θ_1 is the disorientation angle between the slip direction in the grain wherein the crack is initiated and in-depth neighboring grain through which it propagates, Y is the geometric

factor (form function) for a plane edge through-thickness crack with the propagation direction normal to the load direction, $Y = 1.122$, E is the elastic modulus, μ is Poisson's ratio, σ_{-1} is the endurance limit at the symmetrical load cycle, σ_a is the amplitude of cycle stresses applied at a distance from the crack, and N_d is the number of load cycles.

The object of the present study is to develop and verify the fatigue life calculation model in the presence of stress raisers.

Calculation of Fatigue Life to the Crack Initiation in the Presence of Stress Raisers. Formula (1) can be presented as the equation for the fatigue curve to the MSC initiation proposed by Stromeyer [3] already a century ago

$$\sigma_a = \beta N^{-\alpha} + \sigma_{-1}, \tag{7}$$

where β is the fatigue life coefficient, which can be calculated by Eq. (2) and α is the fatigue life exponent. It should be noted that Eq. (7) was proposed to describe the curve of high-cycle fatigue to fracture, i.e., it included both stages of fatigue fracture: nucleation and extension of a fatigue crack, which, as is known, follow different mechanisms. At the same time, under high-cycle fatigue conditions, the ratio between the lengths of fatigue crack nucleation and extension stages for different classes of materials at relatively identical load levels can be essentially different. Thus, for describing these stages, different approaches should be employed. Without regard for this fact, it was long impossible to establish general mechanisms of calculating β and α for different materials and loading conditions. As is seen from Eq. (2), the coefficient β is determined through the elastic parameters E and μ and the microstructure parameters M and ζ, characterizing the texture of the material. The exponent α depends on the energy of packing defects and slip morphology. As was experimentally established by many researchers, $\alpha = 1/2$ for titanium and many other alloys [2].

Hence it follows that such factors as grain sizes and stress concentrations should be allowed for in the calculation of fatigue life to the crack initiation through the change in the endurance limit since σ_a is the amplitude of nominal cycle stresses at a distance from the stress raiser. Thus, in evaluating the durability (or fatigue curves), the endurance limit should be computed considering those factors.

The formula for the calculation of the endurance limit σ_{-1}, including microstructure and stress concentration effects, was proposed [4]

$$\sigma_{-1} = \frac{E\sqrt{b}}{K_t}\sqrt{\frac{1}{\eta d} + \frac{4.5}{\rho}}, \tag{8}$$

where K_t is the theoretical stress intensity factor and ρ is the radius in the stress raiser root.

The grain size d-dependent parameter η is calculated by the formula

$$\eta = \frac{E^2 b}{d}\left(A + B \arctan \frac{E\sqrt{\dfrac{b}{4d}} - A}{B} \right)^{-2}, \tag{9}$$

where $A = (\sigma_f + \sigma_p)/2$, $B = (\sigma_p - \sigma_f)/\pi$, $\sigma_f \cong MG \cdot 10^{-3}$, $G = E/(2(1+\mu))$, d is the grain size, and b is the Burgers vector ($\vec{b}$) module. Formulas (8) and (9) are applicable for "shallow" and "blunt" stress raisers ($K_t < 4$).

For "sharp" and "deep" stress raisers ($K_t > 4$), fatigue strength becomes independent of K_t and is mainly due to the depth of the stress raiser and the threshold stress σ_{th} for physically small or long cracks [5, 6].

Materials and Methods. Verification of the above fatigue life calculation model for the specimens with surface stress raisers made use of high-cycle fatigue test results for Ti–6Al–4V ($\alpha + \beta$)-titanium alloy condensate specimens prepared by the electron beam physical vapor deposition (EBPVD) method [7].

A Ti–6Al–4V condensate, i.e., a vapor cloud condensed on the flat substrate, was obtained from the same but cast alloy. Hence, the composite blanks were produced for condensate/substrate specimens. In the process of
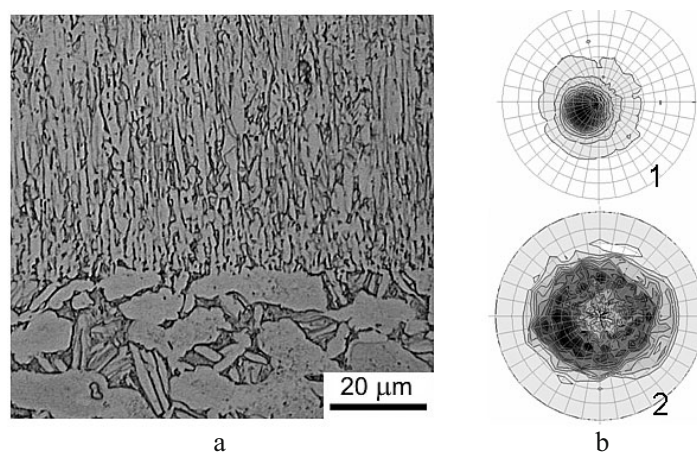
Fig. 1. Structure and texture of an examined material: (a) structure of a Ti–6Al–4V composite specimen (cross-section): top – condensate, bottom – substrate; (b) pole figures (0002) for condensate *1* and substrate *2*, the condensation direction is approximately perpendicular to the Figure plane, which is parallel to the xy plane of the specimens in Fig. 2.
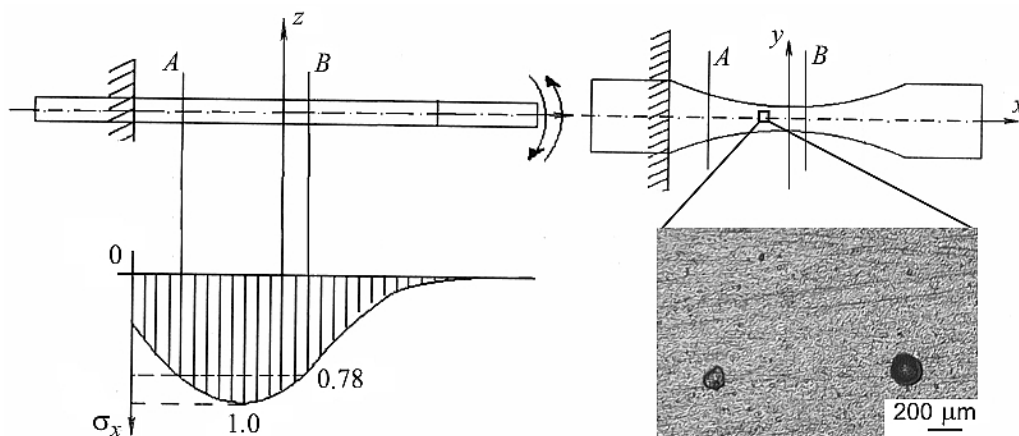

Fig. 2. Fatigue test specimen, its loading scheme, and the stress epure σ_x in relative units. (On the lower right a magnified view of the part of the test portion *AB* surface is presented, dark circles are the defects of different diameter.)

deposition some large drops escape from the melt surface and form columns in the condensate, which grow and reach its surface. Such columns are effective surface stress raisers and affect the fatigue resistance of the condensate with decreasing the endurance limit more than two times in comparison with a similar "conventionally flawless" material and standard cast alloy [7].

The microstructure of composite specimens is shown in Fig. 1. The substrate material exhibits the bimodal structure formed by thermomechanical pretreatment: primary α-phase grains, slightly elongated in the rolling direction, of average sizes of $\sim 10 \times 20\,\mu m$ are separated with the β-phase where secondary α-phase bands are present. The condensate consists of needle α-phase grains (3–4 μm thick and 10–15 μm long), elongated in the growth direction, with β-phase interlayers.

The crystallographic texture was studied by x-ray diffraction on a DRON-3 unit with a specialized goniometer. The pole figures for the condensate and substrate are presented in Fig. 1b. As is seen, the condensate possesses a well-pronounced sharp texture, i.e., a prevailing number of α-phase crystals is oriented so that the base plane (0002) is almost perpendicular to the condensation direction. The substrate texture is not pronounced, blurred, i.e., almost all α-phase grains are disoriented.
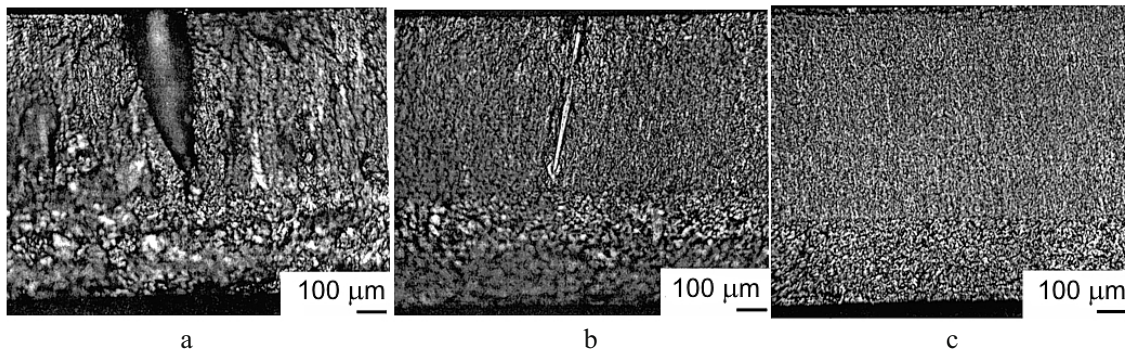
581

Fig. 3. Typical specimen fractures: (a) fracture from the stress raiser $2\rho \cong 200\,\mu\text{m}$; (b) fracture from the stress raiser $2\rho \cong 20\,\mu\text{m}$; (c) fracture initiated on the substrate side.

High-cycle fatigue tests were performed on 30 condensate/substrate specimens. Flat "hour-glass" specimens 1 mm thick and minimum 5 mm wide in the test portion AB (Fig. 2) were tested in symmetrical transverse cantilever bending in the zx plane on an electrodynamic vibration stand with a frequency of $f \cong 350$ Hz.

The moment of MSC propagation to an in-depth neighboring grain was considered the criterion of its initiation one grain size d deep, as was specified by the calculation model [1]. During fatigue tests, this moment was determined by a drastic drop in the resonant frequency Δf of specimen vibrations. A smooth drop in the frequency till this moment was about 0.3% irrespective of load levels. After registering the number of cycles to the crack initiation by a given criterion, the specimen loading was being continued to its final separation into two parts for further examination of fracture surfaces. Moreover, specimens that withstood $N = 10^7$ cycles without fracture were tested at higher stress amplitudes to fracture for detecting the point of fatigue crack initiation. Thus, the nominal stress was evaluated that corresponds to the endurance limit for a respective cross-section.

The examination of specimen fractures demonstrated that all specimens (but three ones) exhibited the crack initiation at the stress raiser/matrix interface on the condensate surface. In the three specimens, the fatigue crack originated on the substrate surface. Therefore, these specimens were considered a "conventionally flawless" condensate, or "smooth" specimens. The most typical fractures are shown in Fig. 3.

It should be noted that examined defects (columns) are not hollow, they are filled with the same deposited Ti–6Al–4V material but with a somewhat different chemical composition and structure. However, porosity around the column results in its squeezing above the specimen surface and further extraction under cyclic loading [7]. Therefore, the above defects were assumed to be hollow in durability calculations.

The measurements of defects (diameter on the surface and depth) demonstrated that in the majority of specimens, the column was positioned at a depth reaching their medial line. Since the specimens were tested in transverse bending and the crack initiation occurred on the surface, the depth of the defect was ignored. Hence the major geometric parameter of those stress raisers responsible for fatigue strength is considered to be their diameter $(2\rho = \sim 20\text{–}300\,\mu\text{m})$ on the specimen surface, measured on fracture photos.

Results of Durability Calculations and Their Discussion. For calculating the durability of a Ti–6Al–4V condensate by the proposed model, the following initial data were used [7]: elastic modulus $E = 1.25 \cdot 10^5$ MPa, Poisson's ratio $\mu = 0.3$, mean diameter of needle grains of the primary α-phase $d = 3.5\,\mu\text{m}$, proportionality limit $\sigma_p = 820$ MPa.

It should be noted that just the primary α-phase is the "weak spot" responsible for the fatigue strength of two-phase $(\alpha + \beta)$-titanium alloys. It should also be mentioned that in such materials the fatigue crack is initiated and extended by the transcrystalline mechanism at room temperature [8, 9].

The following considerations can be applied to determining the parameter b. In the hexagonal close-packed (hcp) crystal of the titanium α-phase (Fig. 4a), slip systems with the Burgers vectors $<\vec{a}>$ (in the $<11\bar{2}0>$ directions and base (0002), prismatic $\{10\bar{1}0\}$, and pyramidal $\{10\bar{1}1\}$ planes) and $<\vec{c}+\vec{a}>$ (in the $<11\bar{2}3>$ directions and
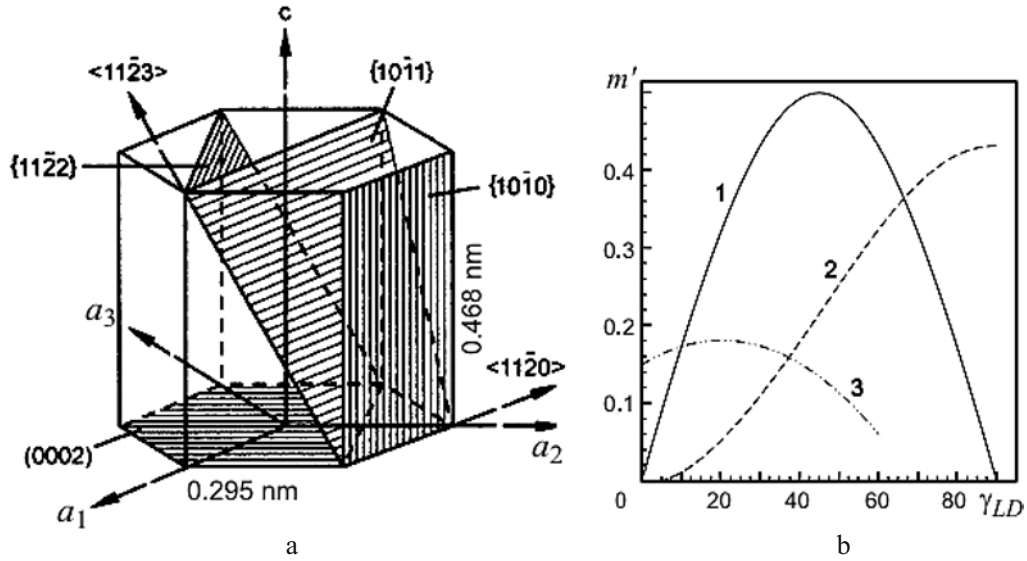
Fig. 4. Slip in α-titanium: (a) single hcp α-titanium cell (basic slip planes are hatched); (b) "normalized" Schmid factor m' vs angle γ_{LD} between the c axis and the load direction for the slip in the base (curve *1*) and prismatic (curve *2*) planes with the direction $<\vec{a}>$ and the pyramidal plane with the direction $<\vec{c}+\vec{a}>$ (curve *3*) [11].

pyramidal $\{11\bar{2}2\}$ and $\{10\bar{1}1\}$ planes) can be activated under cyclic loading. The slip in the prismatic and base planes with the vector $\vec{a}$ is most shear-susceptible since the critical reduced shear stress necessary for the onset of microplastic deformation of the α-titanium crystal in those planes is about 2.6 times smaller than that for the slip activation with the vector $<\vec{c}+\vec{a}>$ in the pyramidal planes [10]. For strongly textured titanium alloys, the predominant grain orientation relative to the load direction should be known, from that the slip system, which would be activated in this case, can be determined.

The "normalized" Schmid factor m' vs angle γ_{LD} between the load direction and c axis for polycrystalline α-titanium is shown in Fig. 4b [11]. Here m' is written as $m' = m(\tau_{\min}/\tau_{<uvtw>\{hkil\}})$, where m is the Schmid factor for a given slip system ($m = 1/M$), $\tau_{\min}$ is the critical reduced shear stress for the most susceptible slip system (base or prismatic), and $\tau_{<uvtw>\{hkil\}}$ is the critical reduced shear stress for a given slip system.

As is seen, when $\gamma_{LD} = 0$–$10°$, the pyramidal slip system $<\vec{c}+\vec{a}>$ would be activated. With an increase in the angle γ_{LD} from 10 to $66.7°$, the base slip system $<\vec{a}>$ is most susceptible. A further increase in the angle from 66.7 to 90° leads to the predominant $<\vec{a}>$ slip in the prismatic plane.

As analysis of the pole figure for an examined condensate demonstrated (Fig. 1a), with the angle between the load direction and c axis close to 90°, for the overwhelming majority of crystals the slip and, correspondingly, nucleation of the fatigue crack occurred in the prismatic planes of some α-phase crystals. Therefore, $b = |\vec{a}|$ was assumed. A small change in the interatomic distance a ($2.95 \cdot 10^{-10}$–$2.93 \cdot 10^{-10}$ m) with an increase in an Al additive from 0 to 12% atomic weight in different titanium alloys are also taken into account [8]. Then for an examined Ti–6Al–4V alloy with 6% Al, $a = 2.94 \cdot 10^{-10}$ m.

Though evaluation of the Burgers vector $\vec{b}$ shows that it is invariant under the line dislocations, they actually change smoothly from the screw to edge one [12]. Therefore, in evaluating b, the correction factor k' should be used ($k' = 1$ for pure screw and $k' = 1 - \mu$ for pure edge ones). Since the dislocation line within the crystal (grain) is between the pure screw and pure edge dislocations, i.e., it is mixed, in this case, the mean k' value was employed. Thus

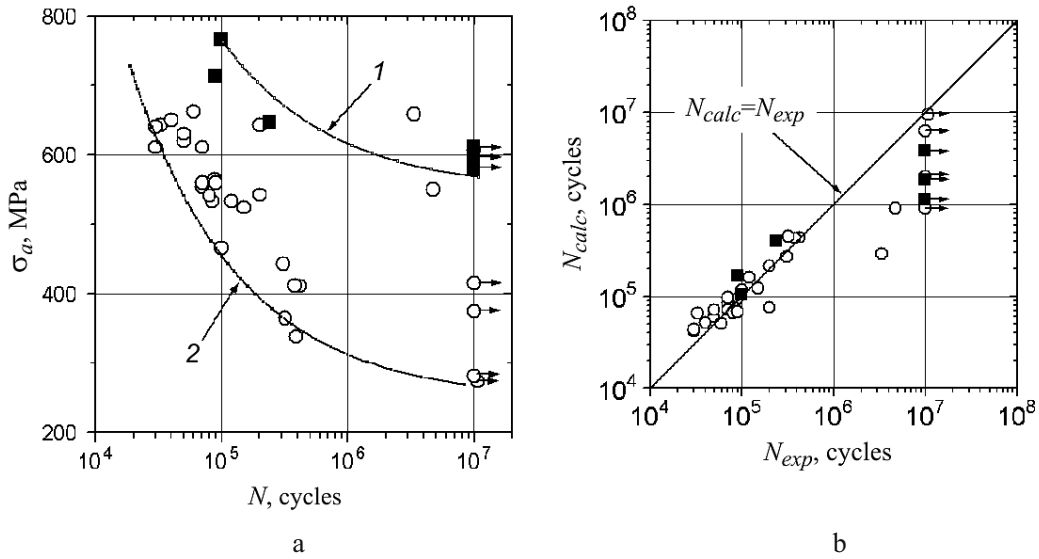$$b = k'a = \frac{2-\mu}{2}a. \tag{10}$$

583

Fig. 5. Comparison of calculation (*1, 2*) and experimental (points) results: (a) [(*1*) "conventionally flawless" condensate ($\rho = \infty$, $K_t = 1$), (*2*) condensate with the stress raiser in the form of a through hole with the diameter of $2\rho = 300\,\mu\text{m}$ ($K_t = 2.676$)]; (b) N_{calc} and N_{exp} are the calculated and experimental durabilities, respectively.

Substituting $\mu = 0.3$ and $a = 2.94 \cdot 10^{-10}$ m in (10), we have $b = 2.5 \cdot 10^{-10}$ m. Based on the above crystallographic orientation of α-grains and also considering that each α-crystal has the three directions $\vec{a}$ in the prismatic $\{10\bar{1}0\}$ planes (Fig. 4a), it can be concluded that on the specimen surface along the perimeter of examined stress raisers ($2\rho = 20$–$300\,\mu\text{m}$), a grain ($d = 3.5\,\mu\text{m}$) can always be found with the most slip-susceptible orientation ($\varphi = \gamma = 45°$). Thus, in accordance with (6), $M = 2$ was taken for calculations, and from a well-pronounced sharp texture (Fig. 1b), the disorientation angle $\theta_1 = 0$. Then the disorientation parameter ζ in accordance with (3) is equal to 0.0125.

Theoretical concentration coefficients K_t for each specimen with the corresponding stress raiser size 2ρ were computed by FEM. The stress raiser was simulated with a through hole [4].

Results of fatigue tests to the crack initiation by the criterion ($\Delta f = 0.3\%$) for Ti–6Al–4V condensate/ substrate specimens in the $\sigma_a - N$ coordinates are presented in Fig. 5a. Here the fatigue curves calculated by the proposed model for a "conventionally flawless" condensate and for a condensate with the stress raiser of the largest diameter. As is seen, practically all experimental data (open circles) that represent specimens with defects of different diameter fall between the fatigue curves. Data obtained for the specimens wherein fracture started on the side of the substrate (dark points) are indicative of a higher fatigue strength of the defect-free condensate in comparison with the substrate. It is quite logical that these points lie below calculated curve *1*.

Calculated and experimental durabilities for examined specimens are compared in Fig. 5b, as is seen, they are in good agreement.

CONCLUSIONS

1. The proposed model for calculating fatigue life to the crack initiation is applicable for
(i) high-cycle fatigue at steady uniaxial symmetrical loads,
(ii) materials with plane slip,
(iii) shallow and blunt surface stress raisers ($K_t < 4$).
2. Such factors as grain sizes and stress concentrations are considered in calculations of fatigue life to the crack initiation through the change in the endurance limit.

3. The calculations by the proposed model would require tensile tests to determine elastic properties (elastic modulus, Poisson's ratio, proportionality limit) as well as analysis of the structure and texture of the initial material to evaluate the size of a grain structure element responsible for the fatigue strength of the material, Taylor factor, Burgers vector.

REFERENCES

1. O. M. Herasymchuk and O. V. Kononuchenko, "Model for fatigue life prediction of titanium alloys. Part 1. Elaboration of a model of fatigue life prior to initiation of microstructurally short crack and a propagation model for physically short and long cracks," *Strength Mater*., **45**, No. 1, 44–55 (2013).
2. K. S. Chan, "Roles of microstructure in fatigue crack initiation," *Int. J. Fatigue*, **32**, 1428–1447 (2010).
3. V. T. Troshchenko and L. A. Sosnovskii, *Fatigue Resistance of Metals and Alloys* [in Russian], Handbook in 2 volumes, Vol. 1, Naukova Dumka, Kiev (1987).
4. O. M. Herasymchuk and O. V. Kononuchenko, "Effect of surface stress concentrators and microstructure on the fatigue limit of the material," *Strength Mater.*, **43**, No. 4, 374–383 (2011).
5. B. Atzori, P. Lazzarin, and G. Meneghetti, "Fracture mechanics and notch sensitivity," *Fatigue Fract. Eng. Mater. Struct.*, **26**, 257–267 (2003).
6. M. Ciavarella and G. Meneghetti, "On fatigue limit in the presence of notches: classical vs. recent unified formulations," *Int. J. Fatigue*, **26**, 289–298 (2004).
7. O. N. Gerasimchuk, G. A. Sergienko, V. I. Bondarchuk, et al., "Fatigue strength of an $(\alpha + \beta)$-type titanium alloy Ti–6Al–4V produced by the electron-beam physical vapor deposition method," *Strength Mater.*, **38**, No. 6, 651–658 (2006).
8. G. Lütjering and J. C. Williams, *Titanium*, Springer, Berlin–Heidelberg–New York (2003).
9. O. M. Herasymchuk, Yu. S. Nalimov, P. E. Markovs'kyi, et al., "Effect of the microstructure of titanium alloys on the fatigue strength characteristics," *Strength Mater.*, **43**, No. 3, 282–293 (2011).
10. O. Herasymchuk and O. Herasymchuk, "Calculation of the critical reduced shear stress for polycrystalline titanium," *Visn. Tern. Nats. Tekhn. Univ*., No. 2 (66), 72–81 (2012).
11. I. Bantounas, D. Dye, and T. C. Lindley, "The effect of grain orientation on fracture morphology during high-cycle fatigue of Ti–6Al–4V," *Acta Mater*., **57**, 3584–3595 (2009).
12. J. P. Hirth and J. Lothe, *Theory of Dislocations*, Wiley, New York (1982).